JOURNAL OF APPLIED ELECTROCHEMISTRY 25 (1995) 770–775

Influence of pH on nickel electrodeposition at low nickel(II) concentrations

W. G. PROUD, E. GOMEZ, E. SARRET, E. VALLES, C. MÜLLER*

Departament de Química Física, Universitat de Barcelona, Martí i Franques 1, 08028 Barcelona, Spain

Received 20 September 1994; revised 24 January 1995

The effect of pH on the nucleation stages of nickel electrodeposition on vitreous carbon has been analysed using low nickel concentrations, without additives. The experimental results indicated that there was a change in the electrochemical response of the system at $4 < pH < 4.5$. A predischarge adsorption ascribed to nickel(II) species was observed with a different surface coverage depending on the pH. Moreover, different inhibition and 3D nucleation processes were detected in varying experimental conditions.

1. Introduction

The fundamental aspects of nickel electrodeposition have been studied by various authors in view of its industrial interest [1–6]. Generally, these studies are performed in 'modified industrial baths' at high nickel concentrations (of the order of 1 M in Ni^{2+}) at low pH (1.5–3), usually in the presence of boric acid and organic additives. Commonly, the aim of the work was to propose mechanisms to explain the effect of pH, additives, anions and nickel concentration on the deposition process on metal surfaces. In particular, Wiart *et al.* [7, 8] have reported many studies using impedance measurements at low pH and high nickel chloride or sulphate concentrations at 50 °C, assuming a mechanism which includes the formation and evolution of a Ni(I) $(OH)_{ads}$ intermediate and also explains the effect of the hydrogen evolution reaction (HER) using H_{ads}, $H_{included}$ and H_2 evolution.

Parallel studies have been performed in order to analyse the first stages of electrodeposition, including the analysis of the formation of critical nuclei. Bozhkov *et al.* [9] using high pH (4–5) and relatively high nickel concentrations (0.2 M) as well as boric acid, demonstrated an initial adatom surface diffusion control of the process in the first stage of nickel formation on vitreous carbon.

To improve our understanding of the contributions of the different solution components and electrochemical parameters to the structure of the electrodeposited nickel films, previous papers from this laboratory [10, 11] reported that, at low nickel concentrations (10^{-2} M) and pH 5, the mechanism of deposition and the morphology of the deposit evolved over a wide range of potentials. Nevertheless, impedance measurements performed in the non-faradaic zone at low Ni^{2+} concentrations and varying pH revealed an adsorption process prior to the faradaic process. The equivalent circuits obtained at pH 5 suggested that the surface was fully covered by an adsorbed layer, while at lower pH the adsorption process was more complex, probably diffusion controlled [12–14]. The average values of the double-layer capacity were in agreement with the assumption of an adsorption process. Taking into account that H_{ads} formation on vitreous carbon was not observed at these potentials in the supporting electrolyte (HER voltammetric current was not obtained), this adsorption behaviour cannot be ascribed to the HER, and a nickel (II) adsorption process may be considered.

Further studies performed at these concentrations at $2 < pH < 5$, without additives, showed a marked change in the electrochemical response at $4 < pH < 4.5$. This sudden change is not described in most papers on nickel electrodeposition, because the authors who used simple unbuffered nickel chloride or sulphate baths used different experimental conditions, working electrode, $[Ni^{2+}]$ and temperature. However, a change in the electrochemical response at pH 4 was observed by Arvia *et al.* in Tafel analysis in more concentrated solutions of nickel which had been deoxygenated with hydrogen [3].

The aim of the study presented here is to analyse the effect of the pH on nickel deposition at low bulk nickel concentrations in relation to nickel concentration and anion type. The substrate used was vitreous carbon, selected to avoid epitaxial growth or UPD phenomena. Simple unbuffered working conditions were selected in order to obtain a reference system to study the influence of boric acid (basic buffer and 'surface active' additive used in plating baths) and other additives, on the deposition process.

2. Experimental details

The chemicals used, $NiCl_2.6H_2O$, $NiSO_4$, and the

* To whom correspondence should be addressed.

0021-891X/93

corresponding sodium salts, were of Merck PA grade; the water was obtained from a MilliQ water purification system. In all cases the counter electrode was a nickel sheet (Johnson Matthey 99.999% pure). For chloride systems, the reference electrode was an Ag/AgCl (Metrohm EA 441/5) mounted in a Luggin capillary containing 1 M NaCl, but all potentials in the text are with respect to SCE; for sulphate systems a mercury sulphate reference (SSE) (Metrohm) was used. The working electrode was a vitreous carbon rotating disc electrode (Tacussel EDI $S = 0.0714\,cm^2$) which permitted rotation speeds up to 5000 rpm or a vitreous carbon bar Metrohm ($S = 0.0314\,cm^2$). The cell had a working capacity of $100\,cm^3$.

The working electrode was polished before each run using different grades of alumina (3.75, 1.78 and 0.3 μm), before being rinsed and finally held in an ultrasonic bath for 1 min.

The concentrations of nickel studied were 1.0, 5.0, 10.0, and 50.0 mM (adjusted to 1 M in chloride or 0.5 M in sulphate with NaCl or Na_2SO_4) at 2.5< pH < 5.5. At these low nickel concentrations, which give a preparation pH of approximately 5, well defined electrochemical behaviour was obtained, which allowed the study of the initial steps of the deposition process [10].

Voltammetric, potentiostatic and galvanostatic measurements were obtained, on a stationary or an RDE electrode using an EG&G potentiostat model 273 controlled by an IBM PS2 model 30.

The deposit morphology was examined with an Olympus PMGC3 metallographic microscope and a Cambridge S-360 scanning electron microscope.

3. Results and discussion

Cyclic voltammetry, pulse techniques and impedance spectra were recorded for a nickel chloride bath in the pH interval 2.5 < pH < 5.5. In all cases, the characteristic hysteresis of a nucleation process was obtained in voltammetry. However, different shape and potential dependences of the voltammetric peaks were observed at pH values lower or higher than approximately 4. (Figs 1 and 2).

At pH > 4 (Fig. 1) a sharp first cathodic voltammetric peak was obtained with an E_{peak} independent of nickel(II) concentration and anion, even at

Table 1. Variation of the first cathodic voltammetric peak potential in nickel deposition (E vs SCE, NaCl supp. electrolyte)

$NiCl_2$ conc./M	Peak potential/mV	
	pH 5	pH 3
10^{-3}	−894	−1290
5×10^{-3}	−894	−1216
10^{-2}	−890	−1198
5×10^{-2}	−896	−1122
$10^{-2} + NiSO_4$	−1310*	−1766*

* E vs SSE Na_2SO_4 supp. electrolyte

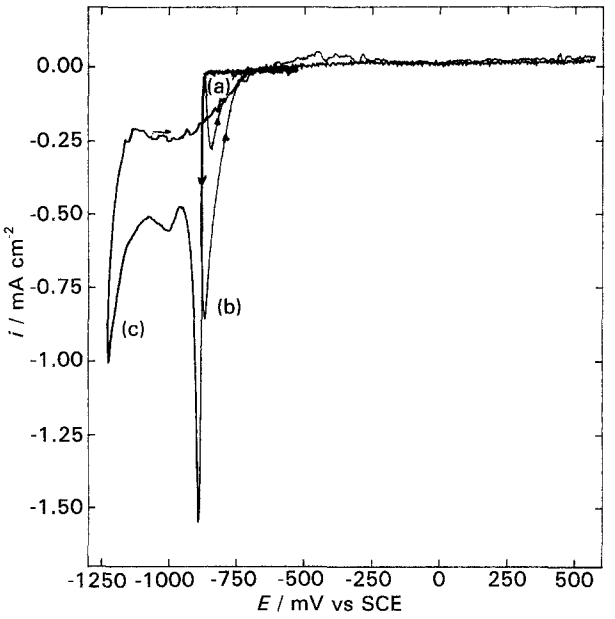

Fig. 1. Cyclic voltammograms for different limit potentials: (a) −875; (b) −885 and (c) −1230 mV. pH 5. 5×10^{-3} M $NiCl_2$ in 1 M NaCl. $v = 10\,mV\,s^{-1}$.

$c > 5 \times 10^{-2}$ M when pH had to be adjusted with ammonia or sodium hydroxide. At these pH values the deposition process was almost irreversible and a small oxidation charge was always obtained in the potential range −1300 to 600 mV vs SCE in the reverse anodic scan.

For pH < 4 (Fig. 2), the deposition process began at more cathodic potentials and an anodic potential shift was observed upon increasing the nickel(II) concentration, or when sodium sulphate was used as the supporting electrolyte (Table 1). Two oxidation peaks corresponding to hydrogenated nickel α-Ni (hydrogen poor) and β-Ni (hydrogen rich) were obtained in the oxidation scan, with the same behaviour as indicated previously [1, 10].

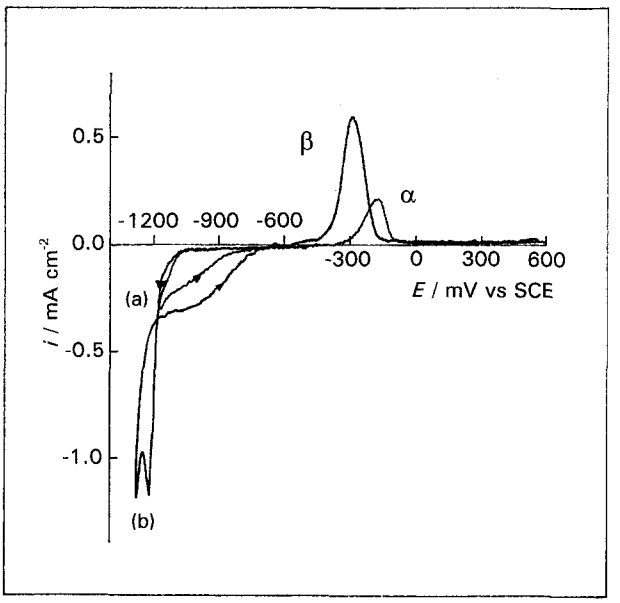

Fig. 2. Cyclic voltammograms for different limit potentials: (a) −1180 and (b) −1200 mV. pH 3. 5×10^{-3} M $NiCl_2$ in 1 M NaCl. $v = 10\,mV\,s^{-1}$.

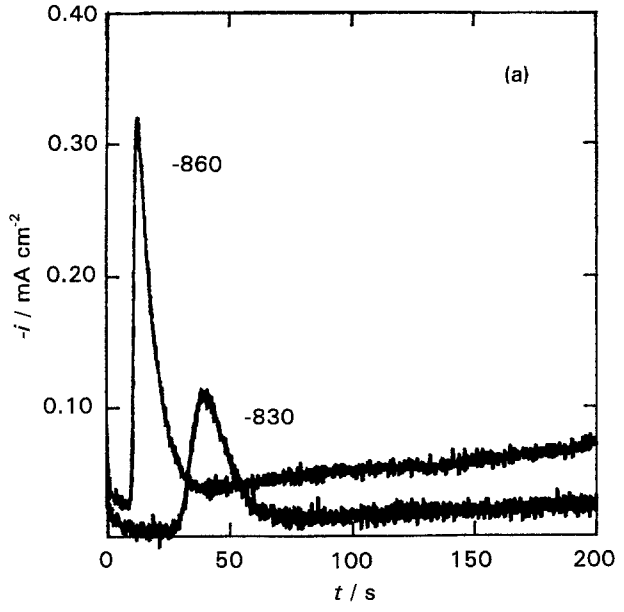

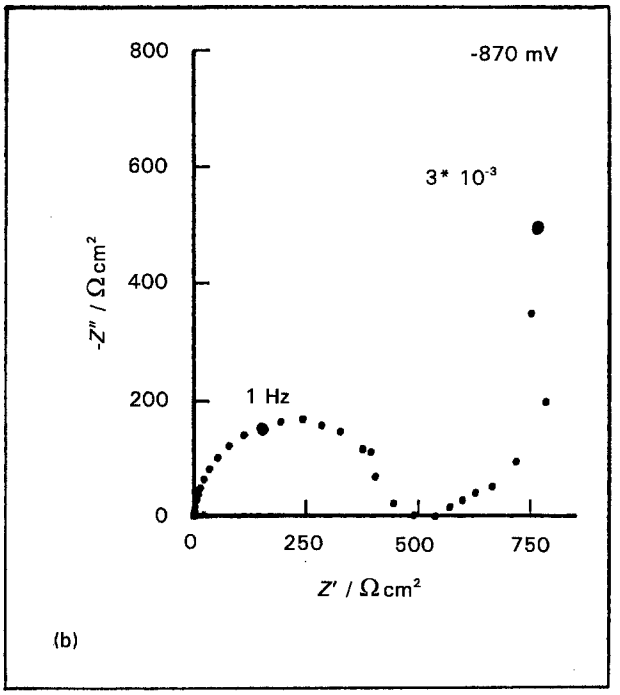

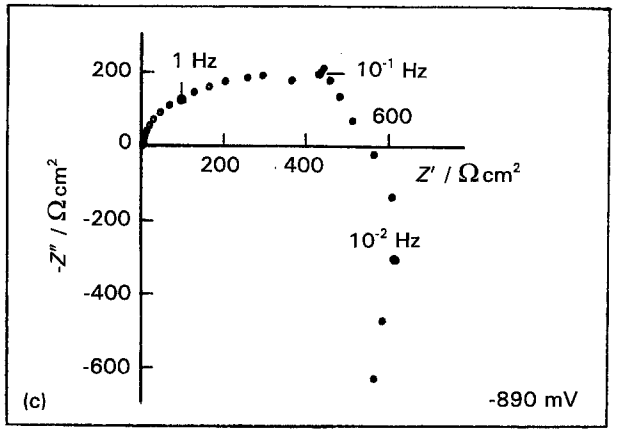

Fig. 3. (a) Potentiostatic current transients for nickel deposition from 0.01 M $NiCl_2$ in 1 M NaCl pH 5, from $E_i = -500$ mV to potentials indicated in the figure. Nyquist impedance plots of (b): 5×10^{-3} M $NiCl_2$ and (c): 0.01 M $NiCl_2$, at potentials indicated in the figure ($S = 0.0714\,cm^2$).

In pulse techniques, in contrast to the quasi-monotonic responses observed at higher nickel concentrations or in the presence of additives [1–3], all the potentiostatic and galvanostatic curves obtained at low nickel concentrations without additives presented several peaks, especially at high pH and low overpotentials.

3.1. *High pH behaviour*

The experimental i against t curves obtained on stationary electrodes at pH 5 showed current peaks in almost all conditions with a measurable induction time at low overpotentials. Nevertheless, the charge corresponding to all these current peaks increased with overpotential.

The potentiostatic peak obtained at low overpotentials (Fig. 3(a)), and the first sharp voltammetric peak (Fig. 1) are related to an inhibition process. SEM analysis of the deposit formed at potential and time conditions corresponding to these peaks showed that the current fell after only a few crystallites were formed, leaving a significant part of the electrode surface free. The charge density calculations performed on these peaks and using SEM micrographs (approximate calculation of number of atoms included in every crystallite: 5×10^9 atoms for a 'medium size' 0.54 μm diameter in Fig. 5 in [10], with 20 crystallites in 358 μm^2), give 6 to 8 mC cm^{-2} in all cases, which is a considerably higher charge than a monolayer (approx 650 μC cm^{-2}). Similarly, the passivation impedance spectra obtained at low overpotentials (Fig. 3(b)) in both chloride and sulphate electrolytes correspond to the same inhibition process.

The desorption behaviour observed in impedance measurements at slightly more cathodic potential (Fig. 3(c)) suggests that this inhibition is produced by a species adsorbed on the freshly deposited nickel crystallites. At this low overpotential, a feasible inhibitor is the adsorbed hydrogen (H^*_{ads}), strongly bonded to the nickel, which has been widely described as an inhibitor of hydrogen evolution and, therefore, probably also modifies the nickel growth process.

However, this inhibition process is not complete and the current never falls to zero. So, the rise in current observed at longer times after the first peak or the second voltammetric peak in Fig. 1 are produced by the evolution, through a 3D growth process leading to coalescence, and the whole surface is covered by a black film of powdered nickel.

The high 'induction time' obtained at these low overpotentials before the evolution of nuclei is more probably due to the slow formation of the critical nuclei, related to the modified electrode surface by the Ni(II) adsorbed layer, than to the very low rate constants for nickel deposition process at these potentials. In agreement with this assumption, when the nucleation process is hindered by adding organic surfactants or hydrogen gas and/or by using forced

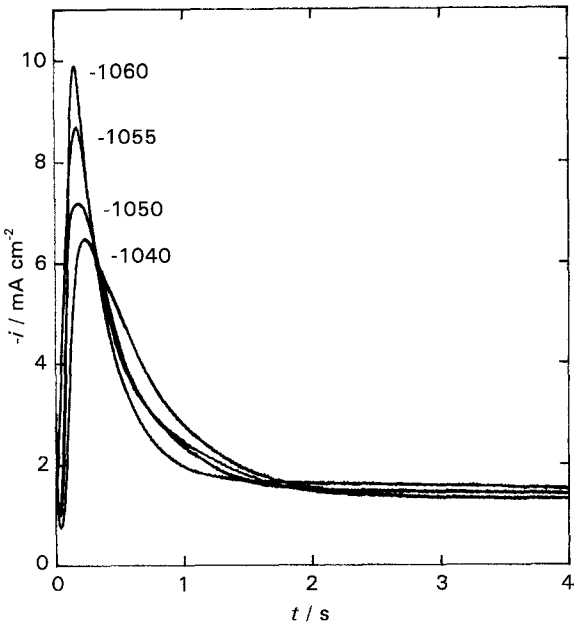

Fig. 4. Potentiostatic current transients for nickel deposition from 0.01 M $NiCl_2$ in 1 M NaCl pH 5, from $E_i = -500$ mV to potentials indicated in the figure ($S = 0.0714\,cm^2$).

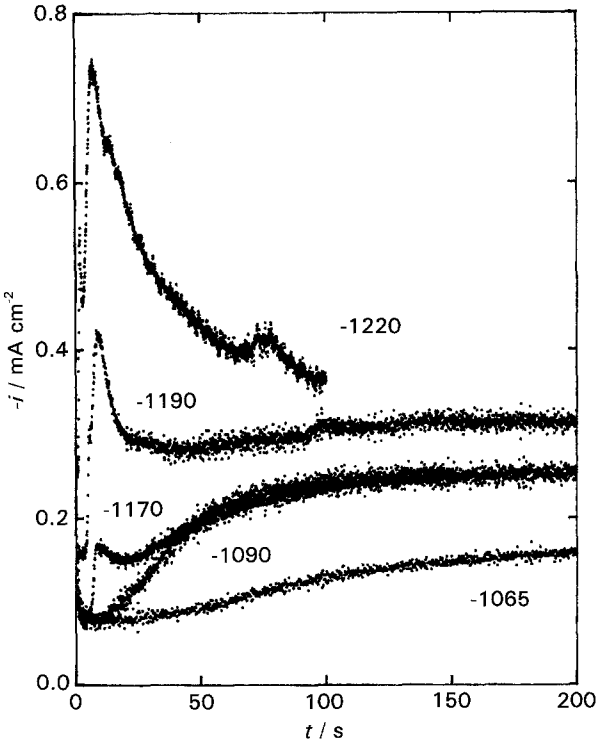

Fig. 5. Potentiostatic current transients in nickel deposition from 5×10^{-3} M $NiCl_2$ in 1 M NaCl pH 3 from $E_i = -500$ mV to potentials indicated in the figure ($S = 0.0714\,cm^2$).

convection (RDE), the induction time is increased [10, 11, 15]. On the other hand, the i against t^3 dependences obtained at low times and the island growth observed with SEM micrographs with crystallites of different size, suggest that the deposit formation takes place through a progressive nucleation with the growth of spherical caps [16–18].

Increasing the overpotential and after the desorption of the inhibitor, a diffusion control appears in the nickel deposition process (Fig. 4) which allows the analysis of the i/t maxima of the potentiostatic transients using Hills model [19]: a bulk diffusion coefficient was calculated ($D = 6.6 \pm 0.4 \times 10^{-6}\,cm^2\,s^{-1}$) which appears to correspond to the nickel$^{2+}_{aq}$ species diffusion. However, in potentiostatic experiments on a RDE at variable rotation speed ω, a second inhibition process is always detected: at long times a decrease is observed in the limiting diffusion current, which falls to approximately 1/10 of its maximum value.

In these experiments, fast hydrogen evolution was detected and a coloured deposit corresponding to $Ni(OH)_x$ precipitate was observed with optical microscopy (OM) due to an increase in the surface pH. As indicated previously [12], a second inhibition impedance spectrum and the corresponding negative slope in the polarization curve were obtained when the coloured film appeared, showing the blocking effect of this precipitate. Upon increasing the overpotential, bubble evolution (forming black holes in the deposit) leading to cracking was observed, and no further inhibition was detected.

3.2. *Low pH behaviour*

At pH < 4, a similar qualitative behaviour was observed in all potentiostatic series (Fig. 5), although the discharge potential varied with nickel concentration, anion and pH.

The most surprising characteristic of these curves is the shape change observed upon increasing the overpotential, as was previously observed at high nickel concentrations at the same pH (pH 3) [15]. While only one monotonic current–time curve with smooth slope appears at low overpotentials and concentrations without induction time (Fig. 5), when the overpotential is raised a new current peak is formed at short times ($E = -1170$ mV).

In all cases, when monotonic potentiostatic curves appeared, isolated hemispherical crystallites were observed in the SEM micrographs, even when the $i_{steady\,state}$ was attained. Stripping analysis at these potentials shows a single anodic peak which can be

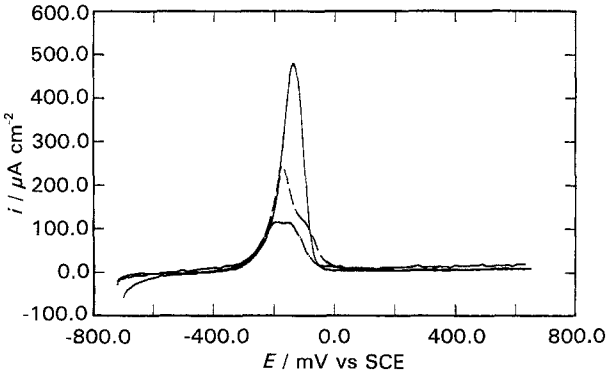

Fig. 6. Potentiodynamic oxidation of nickel deposited under potentiostatic conditions from 5×10^{-3} M $NiCl_2$ in 1 M NaCl pH 3 at: (a) (———) −1105 mV, 200 s; (b) (– –) −1190 mV, 50 s and (c) (– · –) −1230 mV, 50 s. $v = 10\,mV\,s^{-1}$. $S = 0.0714\,cm^2$.

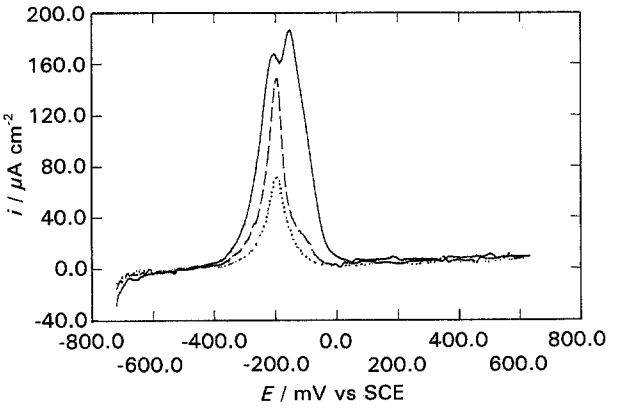

Fig. 7. Potentiodynamic oxidation of nickel deposited under potentiostatic conditions at −1210 mV from 5×10^{-3} M $NiCl_2$ in 1 M NaCl pH 3. Deposition time: (———) 50 s; (– –) 25 s and (···) 15 s. $v = 10\,mV\,s^{-1}$. $S = 0.0714\,cm^2$.

ascribed to α-nickel oxidation (Fig. 6(a)). As usual, the hydrogen-poor form is formed at low overpotentials when little nickel deposit is formed and little hydrogen is produced.

Increasing the overpotential, at low nickel concentrations a charge density of $1300 \pm 100\,\mu C\,cm^{-2}$ which agrees with a film of two atomic layers [9], was obtained for the new peak. This result indicates that the process may take place in two steps: first, the formation of a structure on the whole surface and later, the 3D growth. According to these assumptions, the SEM micrographs of the deposits obtained at different points on the potentiostatic curves showed the initial formation of a compact structure and the posterior growth of new crystallites on the top.

The potentiodynamic oxidation of nickel deposited at these potentials exhibits a split peak which corresponds to the oxidation of both α and β-nickel (Fig. 6(b) and (c)). The voltammetric oxidation of deposits obtained at the same potential and different deposition times (Fig. 7) shows that β-nickel is deposited at short times, up to the peak, while α-nickel appears when the deposition time is increased.

Therefore, the SEM and stripping results show that the peak current obtained at short times at these potentials is due to the coalescence of a β-nickel layer which evolves at longer times to a 3D growth. The formation of this nickel structure on the whole surface of the vitreous carbon electrode enhances the hydrogen evolution at these high potentials and facilitates the deposition of the poorly hydrogenated, but more stable, α-nickel form.

At higher overpotentials (−1220 mV in Fig. 5) the electrochemical behaviour was similar to that of pH 5: the deposition was initially diffusion controlled and an inhibition appeared at long times, produced by a surface pH change favoured by the HER process. The coloured deposit observed in these conditions indicated that nickel hydroxide was locally precipitated, as was observed in other cases, even at lower pH (pH 1.2 in [20]). On the other hand, the high partial current corresponding to this hydrogen evolution produced in all conditions prevents any parameter calculation on potentiostatic curves.

4. Conclusions

The experimental results emphasize that the behaviour of nickel electrodeposition from low nickel concentrations on vitreous carbon is predominantly controlled by the pH of the solution. In chloride and sulphate baths, without additives, a change is observed between pH 4 and 4.5, with an anodic shift in the discharge potentials with increasing pH.

The anomalous current response observed in potentiodynamic and potentiostatic measurements is explained on the basis of different inhibition processes, also observed by impedance measurements. At pH 5 the feasible inhibitors are the H^*_{ads} and $Ni(OH)_x$ species (at low and high overpotentials, respectively), while at pH 3, due to the cathodic shift of the discharge potential, the deposition of nickel is always accompanied by high hydrogen evolution and only the second inhibition process is observed.

Some characteristics of the electrochemical response observed at pH 3 are also due to the formation of α and/or β Ni, species only detected at this pH.

Acknowledgements

The authors are grateful to the DGICYT (Project number PB90-0437) for financial assistance. Grateful thanks are offered to the Ministerio de Educación y Ciencia of Spain for financial support for W.P.

References

[1] M. Fleischmann and A. Saraby-Reintjes, *Electrochim. Acta* **29** (1984) 69, 597.
[2] M. Y. Abyaneh, M. Berkem and M. Fleischmann, *Trans. Inst. Metal Finishing* **58** (1980) 91; **60** (1982) 114.
[3] R. C. V. Piatti, A. J. Arvia and J. Podesta, *Electrochim. Acta.* **14** (1969) 541.
[4] J. Yeager, J. P. Cels, E. Yeager and F. Hovorka, *J. Electrochem. Soc.* **106** (1959) 328.
[5] C. Kollia, N. Spyrellys, J. Amblard, M. Froment and G. Maurin, *J. Appl. Electrochem.* **20** (1990) 1025.
[6] 'Encyclopedia of Electrochemistry of the Elements', vol. 3 (edited by A. J. Bard), Marcel Dekker, New York (1975).
[7] E. Chassaing, M. Joussellin and R. Wiart, *J. Electroanal. Chem.* **157** (1983) 75.
[8] I. Epelboin, M. Joussellin and R. Wiart, *ibid.* **119** (1981) 61.
[9] Chr. Bozhkov, Chr. Tzvetkova, St. Rashkov, A. Budniok and A. Budniok, *ibid.* **296** (1990) 453.
[10] E. Gomez, C. Müller, W. G. Proud and E. Valles, *J. Appl. Electrochem.* **22** (1992) 872.
[11] R. Albalat, E. Gomez, C. Müller, M. Sarret and E. Valles, *ibid.* **21** (1991) 709.
[12] W. G. Proud and C. Müller, *Electrochim. Acta.* **38** (1993) 405.
[13] D. R. Franceschetti and J. R. McDonald, *J. Electroanal. Chem.* **101** (1979) 307.
[14] R. D. Armstrong, R. E. Firman and H. R. Thirsk, *Faraday Discuss. Chem. Soc.* **56** (1973) 244.

[15] E. Gomez, C. Müller, R. Pollina, M. Sarret and E. Valles, *J. Electroanal. Chem.* **333** (1992) 47.
[16] M. Abyaneh, *Electrochim. Acta* **27** (1982) 1329.
[17] R. D. Armstrong, M. Fleischmann and H. R. Thirsk, *J. Electroanal. Chem.* **11** (1966) 208.
[18] M. Y. Abyaneh and M. Fleischmann, *ibid.* **119** (1981) 187, 197
[19] B. R. Scharifker and G. J. Hills, *Electrochim. Acta* **28** (1983) 879.
[20] P. Van Den Brande, A. Dumont and R. Winand, *J. Appl. Electrochem.* **24** (1994) 201.